Helical guided waves in liquid-filled cylindrical shells subjected to static pressurization stress

Brennan Dubuc, Arvin Ebrahimkhanlou, Salvatore Salamone*
Ferguson Structural Engineering Laboratory, Dept. of Civil, Architectural and Environmental Engineering, University of Texas at Austin

ABSTRACT

Helical guided waves in pipelines are studied under the effects of pressurization stresses from a contained liquid. The pipeline is approximated by an "unwrapped" plate waveguide, and a transfer matrix method is used to solve for guided wave velocity and attenuation dispersion curves in a multilayered plate waveguide subject to an arbitrary triaxial state of initial stress. The matrix-based model is able to incorporate both elastic and viscoelastic solid materials, as well as approximate non-uniform distributions in initial stress through the thickness of a waveguide. Experiments on a steel pipe filled with pressurized water are carried out to validate the modeling approach.

Keywords

Acoustoelasticity, viscoelasticity, leaky waves, helical guided waves, transfer matrix method.

1 INTRODUCTION

Guided ultrasonic waves (GUWs) are a potentially high-impact technology for nondestructive evaluation (NDE) methods in various waveguide-like structures. Accordingly, attention to this area has grown in recent years, leading to the development of methods for damage assessment in a number of structural components, such as plates, pipes, rail, &c.[1–4] In general, features like energy velocity and signal attenuation are extracted from GUW signals and processed to aid in the critical tasks of locating and characterizing crucial types of damage. The efficacy of GUWs hinges on their sensitivity to damage. This sensitivity can be significantly affected by variations in normal operating conditions, such as stress distributions, produced either while in service or from manufacturing processes. Knowledge of how these stress distributions affect GUW dispersion characteristics (i.e. wave features) is critical to their successful application.

The effect of initial static stresses on bulk ultrasonic waves is well understood[5–8], yet the influence of these stresses on GUWs is not as developed. Features like wave velocity have been studied in rods[9,10] and plates[11,12] subjected to initial stresses *in vacuo*. A semi-analytical finite element (SAFE) method has been used to study the effect of initial stresses in a waveguide of arbitrary cross-section *in vacuo*, composed of either a single elastic[13] or viscoelastic[14] material. Analyses for layered waveguides have also been formulated[15,16]. However, these analyses have been limited, either to a certain number of layers, or propagation in the direction of a principal axis of initial stress only.

Here, an approach is introduced for eliminating the restrictions stated above that are placed on the initially stressed waveguide. In addition, viscoelastic layers may also be included. The approach provides more freedom for the materials and types of initial/residual stresses that may be studied. The transfer matrix method is used to generate guided wave mode solutions for an initially stressed multilayered waveguide. In addition, due to the convenience of the matrix-based method, the actual layered waveguide may be discretized into sublayers, in order to model initial stresses that vary through the thickness. The transfer matrix method has been chosen for these cases on account of its relatively

* salamone@utexas.edu; phone: +1 (512) 232-3427

Health Monitoring of Structural and Biological Systems 2016, edited by Tribikram Kundu,
Proc. of SPIE Vol. 9805, 98050T · © 2016 SPIE · CCC code: 0277-786X/16/$18 · doi: 10.1117/12.2218897

Downloaded From: http://proceedings.spiedigitallibrary.org/ on 08/29/2016 Terms of Use: http://spiedigitallibrary.org/ss/termsofuse.aspx

higher computation speed, compared to the global matrix method, for a large number of layers. Solutions across real frequency and complex wavenumber are used to describe the effect that initial stresses have on the velocity and attenuation of GUWs. Material absorption and leakage are the two sources of attenuation that are considered.

2 TRANSFER MATRIX METHOD

2.1 BULK WAVES IN A STRESSED LAYER

Matrix-based methods for computing guided wave mode solutions use a partial wave technique to express the guided wave displacements and stresses as a superposition of bulk waves propagating in each layer of a multilayered waveguide. To this aim, the nature of bulk waves propagating in a stressed layer is first analyzed. In the next section, a matrix-based method is then used superimpose these bulk waves and enforce boundary conditions along layer interfaces. This imposition of boundary conditions establishes the existence of guided waves.

The velocity of bulk waves propagating in an initially stressed solid medium vary linearly as the stress is changed[5]. This is known as the acoustoelastic effect.[7] The present approach of accounting for the acoustoelastic effect in triaxially stressed multilayered viscoelastic waveguides expands upon a formulation[11] for Lamb waves in a biaxially stressed plate *in vacuo*. The approach is to model bulk plane wave motion as a time-dependent displacement superimposed on an initial static deformation.[5] The sequence of deformation is composed of three stages: 1) unstrained (natural) stage, 2) initial stage of static deformation, and 3) final stage of wave motion. No plastic deformations are assumed.

The equation of motion, referenced to the natural geometry of a solid medium, for the dynamic incremental displacement **u** (i.e. the wave motion) is[8]

$$A_{\alpha\beta\gamma\delta} u_{\gamma,\beta\delta} = \rho^0 \ddot{u}_\alpha, \tag{1}$$

where a Greek letter following a comma in a subscript denotes partial differentiation with respect to that component of the natural coordinates $\boldsymbol{\xi}$, ρ^0 is the unstrained density, and **A** is expressed

$$A_{\alpha\beta\gamma\delta} = c^{(2)}{}_{\alpha\beta\gamma\delta} - i\omega\tilde{c}_{\alpha\beta\gamma\delta} + c^{(2)}{}_{\beta\delta\varepsilon\zeta} e^i_{\varepsilon\zeta}\delta_{\alpha\gamma} + c^{(2)}{}_{\alpha\beta\varepsilon\delta} e^i_{\gamma\varepsilon} + c^{(2)}{}_{\varepsilon\beta\gamma\delta} e^i_{\alpha\varepsilon} + c^{(3)}{}_{\alpha\beta\gamma\delta\varepsilon\zeta} e^i_{\varepsilon\zeta}. \tag{2}$$

Here, $\mathbf{c}^{(2)}$ and $\mathbf{c}^{(3)}$ are the tensors of second-order and third-order elastic constants, respectively, while $\tilde{\mathbf{c}}$ is the tensor of viscoelastic constants. For an isotropic solid medium, these tensors are[7]

$$\begin{aligned}
c^{(2)}{}_{\alpha\beta\gamma\delta} &= \lambda\delta_{\alpha\beta}\delta_{\gamma\delta} + \mu\left(\delta_{\alpha\gamma}\delta_{\beta\delta} + \delta_{\alpha\delta}\delta_{\beta\gamma}\right), \\
c^{(3)}{}_{\alpha\beta\gamma\delta\varepsilon\zeta} &= \left(2l - 2m + n\right)\delta_{\alpha\beta}\delta_{\gamma\delta}\delta_{\varepsilon\zeta} + \left(m - \tfrac{1}{2}n\right)\left(\hat{\delta}_{\alpha\beta\gamma\varepsilon\delta\zeta} + \hat{\delta}_{\gamma\delta\alpha\varepsilon\beta\zeta} + \hat{\delta}_{\varepsilon\zeta\alpha\gamma\beta\delta}\right) \\
&\quad + \tfrac{1}{4}n\left(\hat{\delta}_{\alpha\gamma\beta\varepsilon\delta\zeta} + \hat{\delta}_{\beta\delta\alpha\varepsilon\gamma\zeta} + \hat{\delta}_{\alpha\delta\beta\varepsilon\gamma\zeta} + \hat{\delta}_{\beta\gamma\alpha\varepsilon\delta\zeta}\right), \\
\tilde{c}_{\alpha\beta\gamma\delta} &= \frac{\tilde{\lambda}}{\omega}\delta_{\alpha\beta}\delta_{\gamma\delta} + \frac{\tilde{\mu}}{\omega}\left(\delta_{\alpha\gamma}\delta_{\beta\delta} + \delta_{\alpha\delta}\delta_{\beta\gamma}\right),
\end{aligned} \tag{3}$$

where λ, μ are the Lamé constants, l, m, n are the Murnaghan constants, and $\tilde{\lambda}$, $\tilde{\mu}$ are the viscoelastic constants. Additionally, $\delta_{\alpha\beta}$ is the Kronecker delta, and $\hat{\delta}_{\alpha\beta\gamma\delta\varepsilon\zeta} = \delta_{\alpha\beta}\left(\delta_{\gamma\delta}\delta_{\varepsilon\zeta} + \delta_{\gamma\zeta}\delta_{\delta\varepsilon}\right)$. $\mathbf{e}^i$ is the infinitesimal static strain resulting from the initial stage of deformation, and is expressed via the Second Piola-Kirchhoff stress $\mathbf{S}^i$ as

Downloaded From: http://proceedings.spiedigitallibrary.org/ on 08/29/2016 Terms of Use: http://spiedigitallibrary.org/ss/termsofuse.aspx

$$e^i_{\alpha\beta} = \frac{1}{2\mu} S^i_{\alpha\beta} - \frac{\lambda}{2\mu(3\lambda + 2\mu)} S^i_{\gamma\gamma} \delta_{\alpha\beta}. \tag{4}$$

In forming the equation of motion, it is assumed that the static stresses in the medium are homogeneous.[8] A small gradually varying inhomogeneity in these stresses, however, does not significantly affect experimental results (see Sec. 4.4).

A constitutive equation for the stress **S** in the incremental stage may also be formed:[11]

$$S_{\alpha\beta} = B_{\alpha\beta\gamma\delta} u_{\gamma,\delta}, \tag{5}$$

where **B** is expressed

$$B_{\alpha\beta\gamma\delta} = c^{(2)}{}_{\alpha\beta\gamma\delta} - i\omega\tilde{c}_{\alpha\beta\gamma\delta} + c^{(2)}{}_{\alpha\beta\varepsilon\delta} e^i_{\gamma\varepsilon} + c^{(3)}{}_{\alpha\beta\gamma\delta\varepsilon\zeta} e^i_{\varepsilon\zeta}. \tag{6}$$

The tensors **A** and **B** reduce to a linear viscoelastic form when the initial stresses vanish.

To simplify the calculation of these tensors, they are first calculated using the principal initial strains, where they are given a special identification as $\mathbf{A}'$ and $\mathbf{B}'$. Afterward, if the principal initial strain axes $\boldsymbol{\xi}'$ do not align with the natural geometry $\boldsymbol{\xi}$, $\mathbf{A}'$ and $\mathbf{B}'$ may be rotated as

$$A_{\alpha\beta\gamma\delta} = a_{\alpha\lambda} a_{\beta\mu} a_{\gamma\nu} a_{\delta\tau} A'_{\lambda\mu\nu\tau}; \quad B_{\alpha\beta\gamma\delta} = a_{\alpha\lambda} a_{\beta\mu} a_{\gamma\nu} a_{\delta\tau} B'_{\lambda\mu\nu\tau}, \tag{7}$$

where the direction cosine between ξ_α and ξ'_β is denoted $a_{\alpha\beta}$.

A plane wave in the ξ_1 - ξ_3 plane is now assumed as a solution to the equation of motion:[17]

$$u_\alpha = U_\alpha \exp[ik(\xi_1 + z\xi_3) - i\omega t], \tag{8}$$

where U_α is the amplitude of the wave motion, k is the wavenumber in the ξ_1 direction, z is the ratio of the wavenumbers in the ξ_3 and ξ_1 directions, and ω is the angular frequency. An eigenvalue problem is formed in the displacement amplitudes,

$$\mathbf{K}(\omega, k, z)\mathbf{U} = \mathbf{0}, \tag{9}$$

where

$$K_{\alpha\beta}(\omega, k, z) = A_{\alpha 1\beta 1} + (A_{\alpha 1\beta 3} + A_{\alpha 3\beta 1}) z + A_{\alpha 3\beta 3} z^2 - \rho^0 \left(\frac{\omega}{k}\right)^2 \delta_{\alpha\beta}. \tag{10}$$

Downloaded From: http://proceedings.spiedigitallibrary.org/ on 08/29/2016 Terms of Use: http://spiedigitallibrary.org/ss/termsofuse.aspx

The eigenvalues of $\mathbf{K}(\omega,k,z)$ describe a set of three upward and downward propagating bulk plane waves. The displacement polarizations of these waves are in general coupled, and this behavior resembles wave propagation in anisotropic solid media. It is thus convenient to work with amplitude ratios for the ξ_2 and ξ_3 displacements as[11,17]

$$V_q = \frac{U_{2q}}{U_{1q}}; \quad W_q = \frac{U_{3q}}{U_{1q}}, \quad q = 1,2,\cdots,6 \quad \text{(no sum)}. \tag{11}$$

Here, q is an index that identifies each of the bulk plane waves. The first subscript on $U_{..}$ denotes the direction component, and the second, q, indicates the bulk wave.

2.2 MULTILAYERED WAVEGUIDE ASSEMBLY

A matrix-based method is now used to generate guided wave solutions for a multilayered waveguide. This is done by combining the bulk waves of each layer into an eigenvalue problem, which is accomplished by imposing continuity in the incremental stresses and displacements along layer interfaces. It is assumed that no discontinuities exist along these interfaces after the initial deformation (i.e. before the wave motion takes place). The transfer matrix method is used here in order to increase the computational speed when the waveguide is composed of a large number of layers.

Layer interfaces are horizontal planes defined by $\xi_3 = \text{const.}$ The natural coordinates of each layer are designed to coincide, although their principal strain axes may differ. In the nth layer the displacements and stresses at a horizontal plane (defined by $\xi_3 = \text{const.}$), from the superposition of all bulk waves in the layer, can be expressed

$$\begin{bmatrix} u_1 & u_2 & u_3 & S_{31} & S_{32} & S_{33} \end{bmatrix}^T = \mathbf{DZ}(\xi_3)\begin{bmatrix} U_{11} & \cdots & U_{16} \end{bmatrix}^T \exp(ik\xi_1 - i\omega t). \tag{12}$$

Because the harmonic terms on the r.h.s are shared, they may be ignored while solving the eigenvalue problem. Here,

$$\mathbf{Z}(\xi_3) = \begin{bmatrix} \exp(ik\xi_3 z_1) & & & (0) \\ & \exp(ik\xi_3 z_2) & & \\ & & \ddots & \\ (0) & & & \exp(ik\xi_3 z_6) \end{bmatrix}, \tag{13}$$

where z_q is the ratio of wavenumbers for the qth bulk wave, and

$$\mathbf{D} = \begin{bmatrix} 1 & V_1 & W_1 & P_{11} & P_{21} & P_{31} \\ \vdots & \vdots & \vdots & \vdots & \vdots & \vdots \\ 1 & V_6 & W_6 & P_{16} & P_{26} & P_{36} \end{bmatrix}^T \tag{14}$$

is called the field matrix for the nth layer. Eq. (5) has been used to produce

$$P_{\alpha q} = ik\left(B_{\alpha 3\gamma 1} + z_q B_{\alpha 3\gamma 3}\right)\frac{U_{\gamma q}}{U_{1q}} \quad (\text{sum on } \gamma). \tag{15}$$

Downloaded From: http://proceedings.spiedigitallibrary.org/ on 08/29/2016 Terms of Use: http://spiedigitallibrary.org/ss/termsofuse.aspx

Assigning the ξ_3 origin of each layer along its lower interface, the quantities along the upper and lower interfaces are be related by

$$\begin{bmatrix} u_1 & \cdots & S_{33} \end{bmatrix}_{\text{top}}^T = \mathbf{L}_n \begin{bmatrix} u_1 & \cdots & S_{33} \end{bmatrix}_{\text{bot.}}^T, \tag{16}$$

where $\mathbf{L}_n = \mathbf{DZ}(\xi_3 = d)\mathbf{D}^{-1}$ is called the layer matrix for the nth layer, and d is the layer thickness. Continuing the process, the quantities along the final M^{th} interface are related to those along the first as

$$\begin{bmatrix} u_1 & \cdots & S_{33} \end{bmatrix}_M^T = \mathbf{Y} \begin{bmatrix} u_1 & \cdots & S_{33} \end{bmatrix}_1^T, \tag{17}$$

where $\mathbf{Y} = \mathbf{L}_N \mathbf{L}_{N-1} \cdots \mathbf{L}_1$ is called the system matrix of the N-layered waveguide.

The eigenvalue problem in $\mathbf{Y}$ may now be solved for the case of a layered waveguide in vacuum by requiring the stresses to vanish along the outer interfaces. If the waveguide is bordered by halfspaces, the eigenvalue problem is formed by requiring that only the outward propagating bulk waves exist in the halfspaces.[18] For this case, the 1st and M^{th} interface quantities are expressed in terms of outgoing wave amplitudes in the halfspaces. This reformulation may be expressed as

$$\begin{bmatrix} U_{11} & \cdots & U_{16} \end{bmatrix}_{\text{t}}^T = \mathbf{D}_{\text{t}}^{-1} \mathbf{Y} \mathbf{D}_{\text{b}} \begin{bmatrix} U_{11} & \cdots & U_{16} \end{bmatrix}_{\text{b}}^T, \tag{18}$$

where $_{\text{t}}$ and $_{\text{b}}$ indicate top and bottom halfspaces. Ordering the wave amplitudes in each halfspace such that those propagating upward (i.e. with a positive real ξ_3 wavenumber) are $\begin{bmatrix} U_{11}, U_{12}, U_{13} \end{bmatrix}$, then $\begin{bmatrix} U_{14}, U_{15}, U_{16} \end{bmatrix}_{\text{t}} = \begin{bmatrix} U_{11}, U_{12}, U_{13} \end{bmatrix}_{\text{b}} = 0$. An eigenvalue problem is then formed for the lower right 3×3 submatrix of the matrix $\mathbf{D}_{\text{t}}^{-1} \mathbf{Y} \mathbf{D}_{\text{b}}$. If there is only one halfspace present, then the reformulation is applied only to that halfspace.

2.3 GUIDED WAVE FEATURES

For guided waves with a complex wavenumber, the imaginary component describes the attenuation along the direction of propagation[18]

$$A'(\omega) = A(\omega) \exp(-k_I r), \tag{19}$$

where k_I is the imaginary component of the wavenumber, $A(\omega)$ is the amplitude of a mode in the frequency domain after it has propagated distance of r, and $A'(\omega)$ is the amplitude after attenuation has been accounted for.

The energy velocity $\mathbf{c}_e$ is the velocity of energy transport for a guided wave packet. It is defined as[19]

$$\mathbf{c}_e = \frac{\langle \mathbf{P}(h,t) \rangle}{\langle E(h,t) \rangle}, \tag{20}$$

where $\mathbf{P}$ is the Poynting vector and E is the total energy. Both $\mathbf{P}$ and E are due to the incremental wave motion only. The operation $\langle \cdot \rangle$ is the average over both one period and the waveguide depth,

Downloaded From: http://proceedings.spiedigitallibrary.org/ on 08/29/2016 Terms of Use: http://spiedigitallibrary.org/ss/termsofuse.aspx

$$\langle \cdot \rangle = \frac{1}{H}\frac{1}{T}\int_0^H \int_0^T (\cdot) dt dh, \tag{21}$$

where T is the period of $(\cdot)$ and H is the thickness of the waveguide.

3 NUMERICAL APPLICATION

3.1 SANDWICH PLATE

An aluminum-epoxy-aluminum sandwich plate is used to demonstrate certain features of guided wave propagation in an initially stressed multilayered viscoelastic waveguide. Before the results are presented, an overview is made of the waveguide that is used to generate numerical results. The waveguide is composed of three layers and bordered by vacuum on each side. Material constants for the layers are defined in Table I (steel and water are used in the experimental section). The third-order elastic constants l,m,n for the epoxy are assumed at 10% of the aluminum values. Fig. 1 provides an illustration of the waveguide. Two different cases of initial stress are analyzed: 1) in-plane uniaxial tension (CS1), and 2) pure flexure superimposed on the tension of the first stress case (CS2). The through-thickness variation in stress caused by the flexure is approximated by discretizing the aluminum layers into five sublayers each, such that each sublayer has a uniform stress distribution. The two stress cases are summarized in Table II. In addition, two different propagation directions are analyzed: 1) parallel to the uniaxial tension (CD1), and 2) perpendicular to the tension (CD2).

	Units: GPa			
	Aluminum	Epoxy	Steel	Water
λ	54.9	5.13	111	2.19
μ	26.5	1.42	82.1	≈ 0
$\tilde{\lambda}$	0	–0.0143+0.00161 i	0	0
$\tilde{\mu}$	0	0.0452–0.00108 i	0	0
l	–252	0.1·(–252)	–461	—
m	–325	0.1·(–325)	–636	—
n	–351	0.1·(–351)	–708	—

TABLE I. Material constants used for numerical results.

	Aluminum (l_1)	Epoxy (l_2)	Aluminum (l_3)
CS1	100	1	100
CS2	150 → 110	1	90 → 50

TABLE II. In-plane normal stresses (s_{11}^i [MPa]) within layers for the two stress cases CS1 and CS2. The symbol "→" indicates that the stresses vary stepwise between the two values.

Dispersion curves for phase velocity c_p, energy velocity c_e, and attenuation k_i, for Lamb-like GUWs in the sandwich plate under different stresses and for different propagation directions are shown in Figs. 2, 3, and 4. Variations in these guided wave features are also shown, with all variations referenced to the unstressed dispersion curves.

Downloaded From: http://proceedings.spiedigitallibrary.org/ on 08/29/2016 Terms of Use: http://spiedigitallibrary.org/ss/termsofuse.aspx

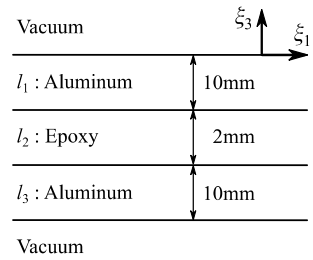

FIG. 1. Sandwich plate waveguide and natural geometry.

Certain characteristics of the attenuative waveguide, like cut-off phase velocities in higher order modes, may be seen in the plots. The directional dependence of the three wave features in the stressed waveguide may be seen in plot (b) of each figure. This directional dependence has been leveraged by other researchers to characterize an unknown stress state in an isotropic plate.[20] Using the presented model, this technique may be used for more general stress states in multilayered plate-like waveguides. It may also be noted that stress and propagation direction cases CS1&CD1 and CS2&CD1 produce nearly identical variations in the wave features for each mode. This indicates that the addition of pure flexure (i.e. an antisymmetric stress distribution through the thickness) to the symmetric waveguide does not alter GUW propagation. This particular conclusion was drawn, based on perturbation theory, for Lamb wave modes in a non-attenuative plate[21]. In this example, it is demonstrated numerically for guided waves in a symmetric multilayered attenuative waveguide.

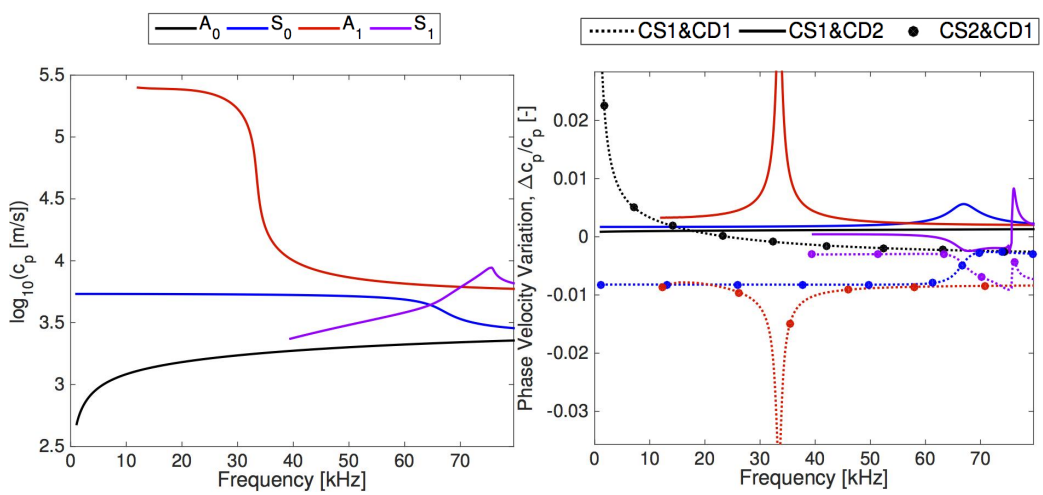

(a) (b)

FIG. 2. (a) Phase velocity dispersion curves for Lamb-like modes under zero stress, and (b) Normalized variations for different stresses and propagation directions. Color indicates the mode and line style indicates the stress/direction condition.

Downloaded From: http://proceedings.spiedigitallibrary.org/ on 08/29/2016 Terms of Use: http://spiedigitallibrary.org/ss/termsofuse.aspx

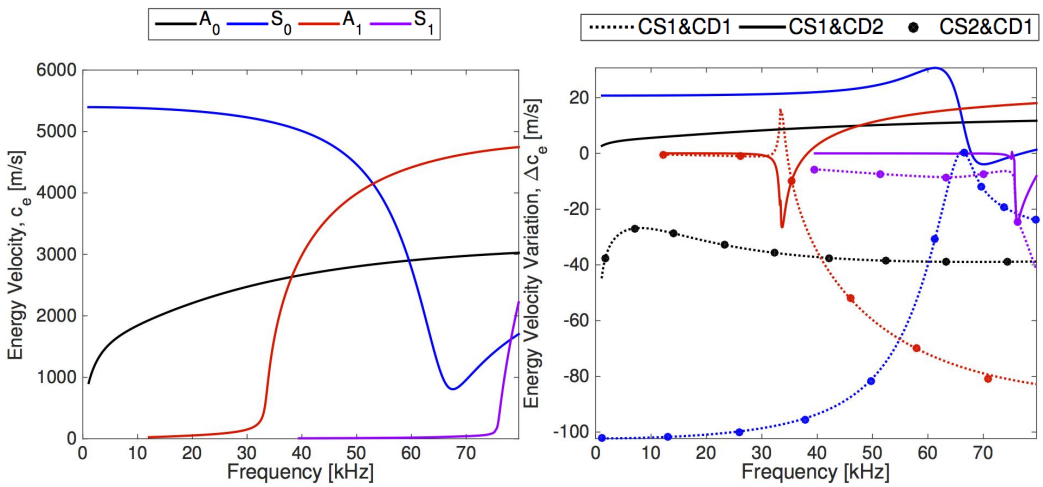

(a) (b)

FIG. 3. (a) Energy velocity dispersion curves for Lamb-like modes under zero stress, and (b) Variations for different stresses and propagation directions. Color indicates the mode and line style indicates the stress/direction condition.

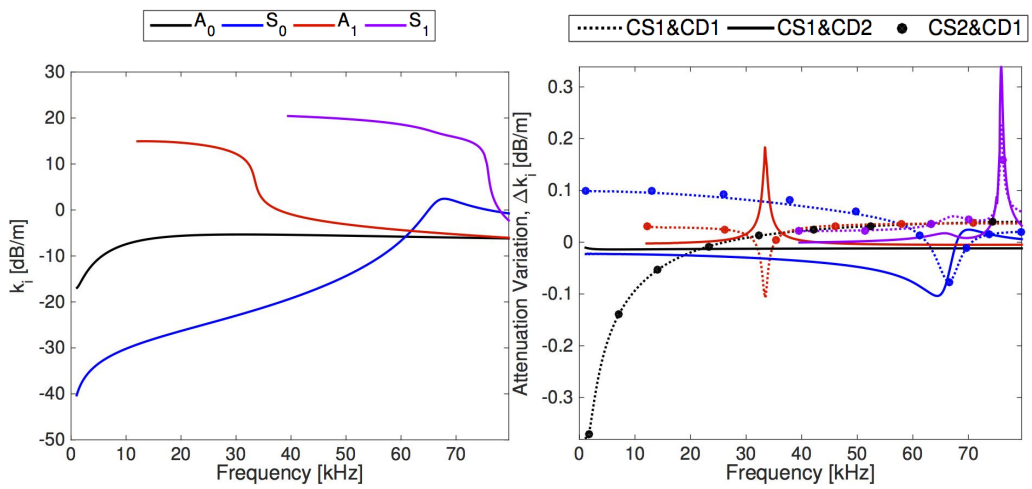

(a) (b)

FIG. 4. (a) Attenuation dispersion curves for Lamb-like modes under zero stress, and (b) Variations for different stresses and propagation directions. Color indicates the mode and line style indicates the stress/direction condition.

4 EXPERIMENTAL STUDY

4.1 HELICAL GUIDED WAVES

The matrix-based method that has been presented is used to predict the effect of pressurization on helical guided waves. Experiments on the effect of stress are performed on a steel pipe filled with pressurized water. For a waveguide with low curvature, such as the large diameter steel pipe, the helical guided wave modes may be approximated by plate wave modes. Due to the geometry of the cylindrical waveguide, multiple helical wave paths exist between a pair of transducers attached to the pipe surface. The additional information provided by multiple paths has recently been exploited for mapping reductions in pipeline wall thickness, using a low density distribution of piezoelectric (PZT) transducers.[22]

Downloaded From: http://proceedings.spiedigitallibrary.org/ on 08/29/2016 Terms of Use: http://spiedigitallibrary.org/ss/termsofuse.aspx

4.2 TEST SETUP

A 3m steel pipe simply supported at its ends and 100% filled with pressurized water is used to experimentally verify the acoustoelastic effect on helical guided waves in a layered, leaky waveguide. The pipe wall has a thickness of d = 2.1mm and inner radius of r_i = 75.1mm. Before ultrasonic testing, temperature equilibrium is reached at 22°C. PZT transducers, with a center frequency f = 400 kHz, are permanently attached to the surface of the pipe. To record the internal pressure, a pressure gauge is instrumented to the pipe. Waveform data is sampled at 10 MS/s using a National Instruments NI PXI system. A 5.5-cycle Hanning toneburst is the excitation waveform. The received signals are averaged 250 times.

Experimental measurements for RMS and energy velocity variations over an internal pressurization range of 0 to 690 kPa are recorded. The pressurization produces hoop and longitudinal stresses in the pipe. The principle initial stresses in terms of the pressurization are

$$S_{11}^{i} = \frac{pr_i}{d}; \quad S_{22}^{i} = \tfrac{1}{2} S_{11}^{i}; \quad S_{33}^{i} = 0, \tag{22}$$

where p is the pressurization value. The principal strain axes of the pipe are assigned as 1) circumferential direction: ξ_1', 2) longitudinal direction: ξ_2', and 3) through-thickness direction: ξ_3'. The natural coordinates $\boldsymbol{\xi}$ for a given helical wave path are thus oriented along a given angle θ in the ξ_1' - ξ_2' plane.

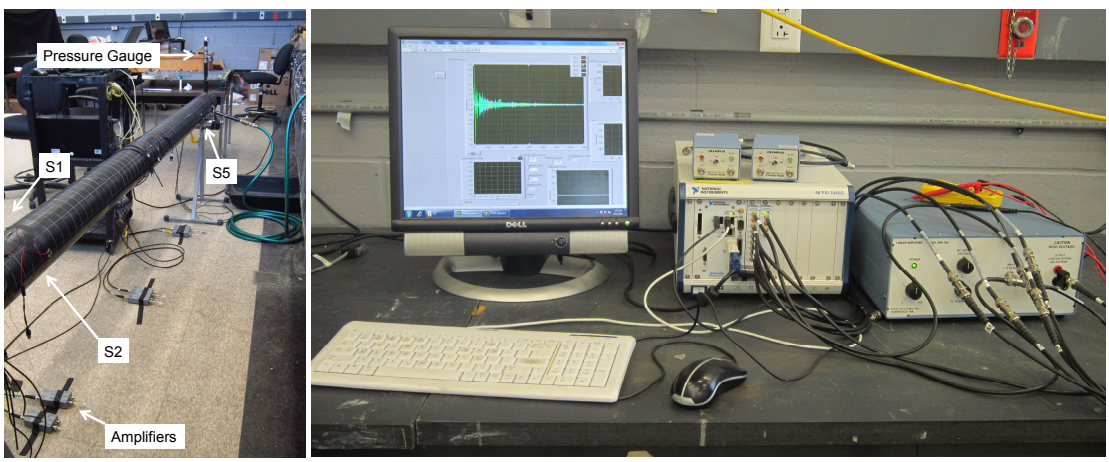

(a) (b)

FIG. 5 Experimental setup (a) for the steel pipe instrumented with PZT transducers and filled with pressurized water. PZT transducers are labeled S1,S2, and S5. Data acquisition system (b).

4.3 ATTENUATION

Changes in RMS are used to describe the variation in attenuation of recorded helical waves. Theoretical predictions for RMS variations under changing pressurization stresses are found using numerical results of imaginary wavenumber for a 2.1mm steel plate bordered on one side by a water halfspace. The initial stresses are those that result from the pressurization in Eq. (22). Material properties for steel and water that are used to generate theoretical dispersion curves are contained in Table I.[23] The water is modeled as a solid with a small shear modulus. The frequency domain of a reference signal measured at a certain propagation distance under zero stress is scaled according to the attenuation dispersion curves for the mode being analyzed. The theoretical prediction for RMS is then calculated after transforming the resultant frequency spectrum into the time domain. Experimental and theoretical RMS variations for the Lamb-like S_0 and A_0 helical wave modes may be found in Fig. 6. As the attenuation variations in the two modes are relatively low at the tested frequency (400 kHz), the fluctuations due to noise are evident in the plots of RMS, even after the signals

Downloaded From: http://proceedings.spiedigitallibrary.org/ on 08/29/2016 Terms of Use: http://spiedigitallibrary.org/ss/termsofuse.aspx

have been postprocessed. It has thus proven difficult to verify these theoretical solutions for variations in guided wave attenuation under changing stress.

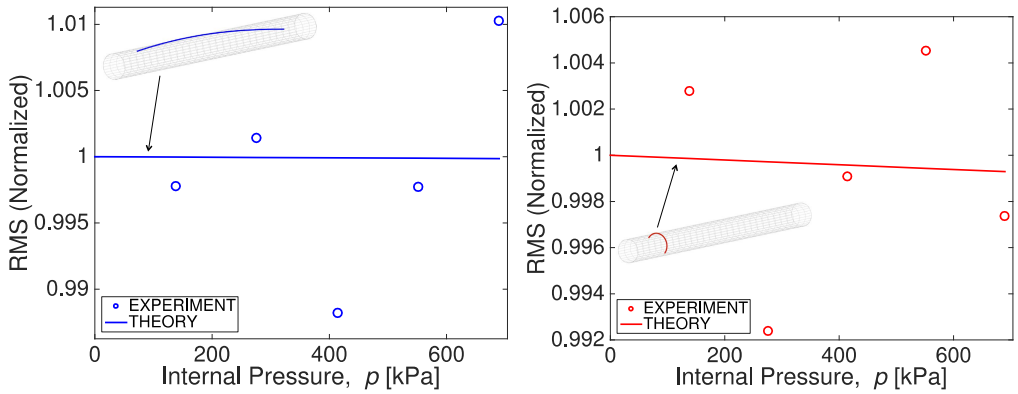

FIG. 6 RMS variations (normalized against the zero pressure state) for S_0 (a) and A_0 (b) in the steel pipe filled with water under increasing pressurization. Helical path S1-S5 is shown for S_0, and S1-S2 for A_0.

4.4 ENERGY VELOCITY

Experimental changes in energy velocity are measured using a cross-correlation method. Results for the Lamb-like S_0 and A_0 modes may be found in Fig. 7. Included in the plot are numerical results for an initially stressed 2.1mm steel plate that is loaded on one side by a water halfspace. At the tested frequency, changes in energy velocity due to the pressure are more noticeable than attenuation. Results for the S_0 mode along two different helical paths illustrate the changes in velocity variation for different propagation orientations relative to the principal initial strains. The paths S1-S2 and S1-S5 are highlighted, due to their large differences in propagation orientation, demonstrating the effect this has on their respective energy velocity variations. Due to large attenuation in the A_0 mode, only the shortest helical path around the pipe is useable.

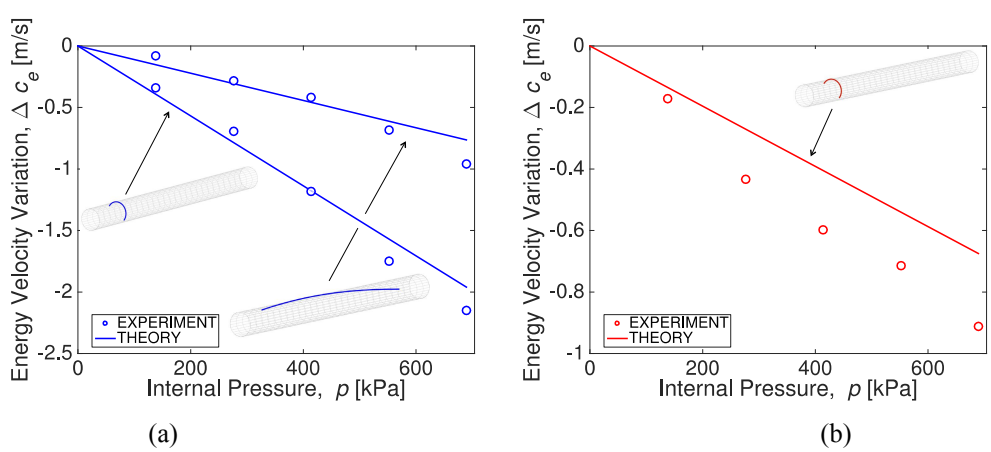

FIG. 7 Energy velocity variations for S_0 (a) and A_0 (b) for the steel pipe filled with water under increasing pressurization. Helical paths S1-S2 and S1-S5 are shown for S_0, and path S1-S2 for A_0.

The helical path S1-S5 is oriented predominantly along the axis of the pipe, and it demonstrates the negligibility of the selfweight stresses when compared to the pressurization. The maximum selfweight stress is on the order of 20% of the maximum pressurization stress.

Downloaded From: http://proceedings.spiedigitallibrary.org/ on 08/29/2016 Terms of Use: http://spiedigitallibrary.org/ss/termsofuse.aspx

5 CONCLUSIONS

A matrix-based approach has been presented for the computation of guided wave dispersion curves in a triaxially stressed plate-like multilayered viscoelastic waveguide. Predictability in energy velocity variations has been demonstrated. As these variations are linear, only simple adjustments are necessary if this effect is to be incorporated into a SHM system. As common GUW-based SHM methods in pipelines depend upon an understanding of wave velocities under idealistic conditions[1,22], the effect of operational stresses may negatively influence these methods if they are not accounted for, depending particularly on the waveguide, mode, and frequency range used. Due to the frequency range evaluated in the experiments, reducing noise and making accurate signal RMS readings was encountered. Further research is necessary in measuring third-order elastic constants for more materials.

6 ACKNOWLEDGMENTS

Funding for this research has been provided by the United States Department of Transportation (DOT), Pipeline and Hazardous Materials Safety Administration's (PHMSA) under the Competitive Academic Agreement Program (CAAP) (#DTPH56-13-H-CAAP03). Any opinions, findings, conclusions or recommendations expressed are those of the author(s) and do not necessarily reflect the views of the PHMSA.

7 REFERENCES

1. Seher, M., Huthwaite, P., Lowe, M. J. S. & Cawley, P. Experimental study of A0 Lamb wave tomography. *Rev. Prog. Quant. NDE* **34,** 245–253 (2015).
2. Ebrahimkhanlou, A., Dubuc, B. & Salamone, S. Damage localization in plate-like structures using guided ultrasonic waves edge reflections. in *10th IWSHM* 2521–2528 (DEStech Publications, Inc., 2015).
3. Moustafa, A. & Salamone, S. Fractal dimension-based Lamb wave tomography algorithm for damage detection in plate-like structures. *J. Intell. Mater. Syst. Struct.* **23,** 1269–1276 (2012).
4. Rizzo, P. *et al.* Ultrasonic guided waves-based monitoring of rail head: Laboratory and field tests. *Adv. Civ. Eng.* **2010,** 1–13 (2010).
5. Hughes, D. S. & Kelly, J. L. Second-Order Elastic Deformation of Solids. *Phys. Rev.* **92,** 1145–1149 (1953).
6. Thurston, R. N. & Brugger, K. Third-order elastic constants and the velocity of small amplitude elastic waves in homogeneously stressed media. *Phys. Rev.* **133,** 1604–1610 (1964).
7. Toupin, R. A. & Bernstein, B. Sound waves in deformed perfectly elastic materials. Acoustoelastic effect. *J. Acoust. Soc. Am.* **33,** 216–225 (1961).
8. Pao, Y.-H. & Gamer, U. Acoustoelastic waves in orthotropic media. *J. Acoust. Soc. Am.* **77,** 806–812 (1985).
9. Mott, G. Elastic waveguide propagation in an infinite isotropic solid cylinder that is subjected to a static axial stress and strain. *J. Acoust. Soc. Am.* **53,** 1129–1133 (1972).
10. Bartoli, I. Structural health monitoring by ultrasonic guided waves. (2007).
11. Gandhi, N., Michaels, J. E. & Lee, S. J. Acoustoelastic Lamb wave propagation in biaxially stressed plates. *J. Acoust. Soc. Am.* **132,** 1284–1293 (2012).
12. Pau, A. & Lanza di Scalea, F. Nonlinear guided wave propagation in prestressed plates. *J. Acoust. Soc. Am.* **137,** 1529–1540 (2015).
13. Chen, F. & Wilcox, P. D. The effect of load on guided wave propagation. *Ultrasonics* **47,** 111–22 (2007).
14. Mazzotti, M., Marzani, A., Bartoli, I. & Viola, E. Guided waves dispersion analysis for prestressed viscoelastic waveguides by means of the SAFE method. *Int. J. Solids Struct.* **49,** 2359–2372 (2012).
15. Biot, M. A. *Mechanics of Incremental Deformation*. (John Wiley & Sons, 1965).
16. Qu, J. & Liu, G. in *Rev. Prog. Quant. NDE* (Thompson, D. O. & Chimenti, D. E.) **17,** 1635–1642 (Plenum Press, 1998).
17. Nayfeh, A. H. & Chimenti, D. E. Free wave propagation in plates of general anisotropic media. *J. Appl. Mech.* **56,** 881–886 (1989).
18. Lowe, M. J. S. Matrix techniques for modeling ultrasonic waves in multilayered media. *IEEE Trans. Ultrason. Ferroelectr. Freq. Control* **42,** 525–542 (1995).
19. Achenbach, J. D. *Wave Propagation in Elastic Solids*. (North Holland Publishing Co., 1973).

Downloaded From: http://proceedings.spiedigitallibrary.org/ on 08/29/2016 Terms of Use: http://spiedigitallibrary.org/ss/termsofuse.aspx

20. Shi, F., Michaels, J. E. & Lee, S. J. In situ estimation of applied biaxial loads with Lamb waves. *J. Acoust. Soc. Am.* **133,** 677–687 (2013).
21. Husson, D. A perturbation theory for the acoustoelastic effect of surface waves. *J. Appl. Phys.* **57,** 1562–1568 (1985).
22. Dehghan-Niri, E. & Salamone, S. A multi-helical ultrasonic imaging approach for the structural health monitoring of cylindrical structures. *Struct. Heal. Monit.* **14,** 73–85 (2014).
23. Muir, D. D. One-sided ultrasonic determination of third order elastic constants using angle-beam acoustoelasticity measurements. (2009).

Downloaded From: http://proceedings.spiedigitallibrary.org/ on 08/29/2016 Terms of Use: http://spiedigitallibrary.org/ss/termsofuse.aspx